Research Square

Preprints are preliminary reports that have not undergone peer review.
They should not be considered conclusive, used to inform clinical practice,
or referenced by the media as validated information.

Contrasting Triggering and Maintenance Mechanisms of Two Squall Lines and Extreme Gale Causes under a Common Cold Vortex

Jiangshan Luo
Qingdao Meteorological Bureau
Fujing Wan
1005418392@qq.com

Qingdao Meteorological Bureau
Jian Li
East China Phased Array Weather Radar Application Joint Laboratory

Research Article

Keywords: Cold Vortex, Squall Line, Extreme Gale, Vertical Wind Shear, RKW Theory

Posted Date: July 31st, 2026

DOI: https://doi.org/10.21203/rs.3.rs-10456307/v1

License: This work is licensed under a Creative Commons Attribution 4.0 International License.
Read Full License

Additional Declarations: No competing interests reported.

Contrasting Triggering and Maintenance Mechanisms of Two Squall Lines and Extreme Gale Causes under a Common Cold Vortex

JIANGSHAN LUO,[1] FUJING WAN,[1, 2,*], JIAN LI [2, 3]

Abstract—Using data from automatic weather stations, Doppler radar, and ERA5 reanalysis, this study examined the differences in triggering and maintenance mechanisms, as well as the origins of extreme gales, between two squall lines that impacted the region spanning southern North China to the Huanghuai area on June 13, 2022. This event unfolded against the backdrop of a Northeast China Cold Vortex. Presence of strongly unstable stratification, marked by cold and dry mid-level air juxtaposed with warm and moist low-level air, created conducive conditions for convective outbreaks. The triggering mechanisms of the two squall lines diverged. Squall Line I was clearly triggered by a combination of factors: a synoptic-scale shear line, a mesoscale surface vortex, and its associated convergence line. Subsequently, it was organized through convective merger processes. In contrast, Squall Line II emerged without significant synoptic-scale forcing. Its initial convection was triggered by the thermal effects of the Taihang Mountains' topography and was later organized by the convergence line formed through the interaction between low-level easterly winds and the terrain, coupled with frontogenetic dynamic forcing. Significant differences were also observed in their maintenance mechanisms. Squall Line I exhibited a long lifespan and wide impact range, maintained by a sustained equilibrium between the propagation speed of the cold pool and low-level vertical wind shear. In contrast, Squall Line II had a short lifespan and small scale, primarily due to a rapid disruption of the balance between these two factors. Furthermore, the physical mechanisms underlying the extreme gales varied. For Squall Line I, the gales were predominantly driven by outflow generated by the strong pressure gradient associated with a large-scale, high-intensity cold pool. For Squall Line II, localized extreme gusts were more closely linked to the small- to medium-scale bow echo structure, the strong rear-inflow jet that developed within it, and the dynamic processes associated with the mesoscale vortex.

Key words: Cold Vortex, Squall Line, Extreme Gale, Vertical Wind Shear, RKW Theory

1. Introduction

* Corresponding author.

[1] Qingdao Meteorological Bureau, Qingdao, China. E-mail: luo_jsh@126.com; 1005418392@qq.com

[2] East China Phased Array Weather Radar Application Joint Laboratory, Shanghai, China. E-mail: 1005418392@qq.com; 1767469080@qq.com

[3] Meteorology Center of East China Regional Air Traffic Management Bureau of Civil Aviation of China, Shanghai, China. E-mail: 1767469080@qq.com

A squall line, a mesoscale weather system, frequently brings about disastrous weather phenomena, including high winds, tornadoes, hail, and short-duration heavy rainfall, thus posing substantial destructive threats. Understanding the mechanisms underlying its initiation, organization, and propagation remains a formidable challenge in operational forecasting. The initiation and organization of squall lines are intricately linked to mesoscale disturbances, such as surface wind convergence lines, fronts, mid-level jets, and topographic effects (Meng et al., 2013; French & Parker, 2014; Zhou et al., 2020). Boundary-layer convergence lines are pivotal in triggering and intensifying severe storms like squall lines (Trier, 2003; Weckwerth & Romatschke, 2019; Schumacher & Rasmussen, 2020; Luo et al., 2014, 2017; Liu et al., 2023). During squall line evolution, the interaction between environmental vertical wind shear and the cold pool is a critical mechanism governing the maintenance, development, intensification, and propagation of squall lines and other convective systems (Abramian et al., 2022; Song et al., 2005; Gebauer et al., 2018; Du & Chen, 2019). Beyond vertical wind shear and the cold pool, factors such as static stability, boundary-layer convergence lines, low-level moisture content, and energy conditions also significantly influence the development and maintenance of squall lines (Carbone et al., 1990; Reif & Bluestein, 2017; Hong et al., 1999; Wan et al., 2024).

High winds represent one of the most hazardous weather phenomena associated with squall line systems. The thunderstorm high pressure resulting from pressure surges as a squall line passes, the associated strong pressure gradient, the rapid movement of the squall line, and the rear-inflow jet all contribute to surface gales. The surface cold pool plays a crucial role in generating damaging winds in squall lines and is a key factor in the development of extreme thunderstorm gales (Wan et al., 2021). Studies have demonstrated that strong thunderstorm high pressure, the intense pressure gradient ahead of the high pressure system, and the rapid movement of strong squall lines are direct causes of high wind generation (Hitchcock & Schumacher, 2020; Parker, 2021; Peters & Schumacher, 2014; Zhang et al., 2023).

From morning to night on June 13, 2022, influenced by a Northeast China Cold Vortex, the region from southern North China to the Huanghuai area experienced a rare double-squall-line weather event, accompanied by widespread thunderstorm gales, short-duration heavy rainfall, and localized hail. A notable feature of this event was the successive development of two organized squall line systems within two hours at the base of the cold vortex, significantly complicating forecasting and warning efforts. While previous studies (Huang et al., 2025) have explored convective initiation and organization in this event, a quantitative description of squall line maintenance mechanisms remains absent. In this study, ‘damaging gales’ is defined as surface winds with Beaufort force $\geqq$ 8 ($\geqq$17.2 m/s), the threshold for wind damage in China's operational wind warning standard, while ‘extreme gales’ refers to Beaufort force $\geqq$ 10 ($\geqq$ 24.5 m/s).

This study aims to delve into the following scientific questions: First, under the same Northeast China Cold Vortex background, how did environmental conditions support the successive triggering of the two squall lines? Second, what are the essential differences in the initiation and maintenance mechanisms between the two squall lines, and which key environmental factors and dynamic processes led to their significant differences in intensity, duration, and impact range? Finally, what are the differences in the physical mechanisms responsible for the extreme gale events associated with the two

squall lines? Addressing these questions holds substantial scientific significance and practical value for enhancing forecasting and warning capabilities for similar events. To this end, this study presents an observational and diagnostic analysis of the two squall lines, quantifying the key physical parameters that distinguish their behaviors and providing a diagnostic framework that can serve as a reference for future observational and modeling studies in this region.

2. Data and Methods

2.1. Data

To elucidate the multi-scale characteristics of the double-squall-line event, this studyemployed multi-source observational and reanalysis data. The datasets employed are detailed as follows:

Surface observational data: Hourly data from national meteorological observation stations and regional automatic weather stations are utilized. These data serve multiple purposes: analyzing the evolution of mesoscale surface systems (e.g., convergence lines, cold pools), calculating meteorological variables (e.g., divergence, frontogenesis function), and validating reanalysis fields.

Radar data: Base data from multiple S-band Doppler weather radars in North China are employed. Products such as composite reflectivity factor and radial velocity are analyzed to track the three-dimensional structure of convective systems and identify features, including squall lines, bow echoes, and mesocyclones.

Reanalysis data: Hourly ERA5 reanalysis data from the European Centre for Medium-Range Weather Forecasts (ECMWF), with a horizontal resolution of 0.25° × 0.25°, are primarily used to analyze the synoptic-scale circulation background, compute thermodynamic and dynamic parameters, and provide the environmental background field. This resolution is adequate for representing the large-scale thermodynamic environment (CAPE, vertical wind shear) and the synoptic-scale circulation, but is insufficient to resolve finescale mesoscale features such as gust fronts and narrow convergence lines. To resolve these, we rely primarily on Doppler radar observations and surface automatic weather station data. All mesoscale features discussed in this study—including convergence lines, gust fronts, cold pool boundaries, and bow echo structures — are identified from radar reflectivity and surface wind observations, not directly from ERA5 grids. ERA5 is used only to provide the thermodynamic context for these radar-observed features. The application of ERA5 reanalysis data in diagnosing extreme weather events has been widely validated in recent regional studies (Yan et al., 2022; Zhao et al., 2025), further supporting the reliability of the dataset used in this study.

Radiosonde data: Observational data from conventional radiosonde stations are employed to analyze the thermal and dynamic stratification characteristics prior to convection initiation.

2.2. Methods

This study integrates diagnostic analysis and theoretical models to focus on the initiation and maintenance mechanisms of the two squall lines, as well as the causes of the associated high winds.

Mesoscale frontogenesis diagnosis: To quantitatively describe the mesoscale dynamic forcing process, the frontogenesis function at 925 hPa is calculated using ERA5 reanalysis data, as defined by Petterssen (1956), and is calculated as shown in Eq. (1).

$$F=\frac{1}{2}|\nabla\theta|[D\cos(2\beta)-\delta] \quad (1)$$

In Eq. (1), D represents horizontal wind shear (deformation term), δ is divergence, β is the angle between the axis of dilation and the isentropes, and θ is potential temperature. F>0 indicates frontogenesis, while F<0 indicates frontolysis. The evolution of the frontal zone is further analyzed in conjunction with the frontal zone of equivalent potential temperature and temperature advection.

Rotunno-Klemp-Weisman (RKW) theory analysis: To quantitatively evaluate the maintenance mechanism of the squall lines, key parameters characterizing cold pool intensity are calculated based on the RKW theory. The propagation speed of the cold pool boundary (C) can be approximated as the propagation speed of a two-dimensional density current (Benjamin, 1968). Assuming a cold pool depth H and a perturbation potential temperature $\Delta\theta$, the propagation speed of the cold pool boundary can be estimated using the surface pressure perturbation Δp induced by the cold pool, and is calculated as shown in Eq. (2).

$$C^2=2g\frac{-\Delta\theta}{\bar{\theta}}H=2g\frac{\Delta\rho}{\bar{\rho}}H=2\frac{\Delta p}{\bar{\rho}} \quad (2)$$

In Eq. (2), Δp is the pressure difference between the inside and outside of the cold pool, representing the surface pressure perturbation caused by the cold pool, and $\bar{\rho}$ is the mean density of surface air. Simultaneously, the environmental vertical wind shear between 0 and 3 km (denoted as $\Delta U_{0\text{-}3\ km}$) is calculated. By computing the ratio of cold pool intensity to environmental vertical wind shear ($C/\Delta U_{0\text{-}3\ km}$), the interaction between the cold pool and vertical wind shear can be quantitatively diagnosed. A ratio close to 1 indicates a balance between the two, which is conducive to squall line maintenance; a ratio deviating from 1 suggests the disruption of this balance (Weisman & Rotunno, 2004).

3. Case Overview

On June 13, 2022, a severe convective weather event, triggered by two squall lines, swept across North China and the Huanghuai region under the influence of a Northeast China Cold Vortex. This event impacted a wide area, bringing hail, thunderstorm gales, and short-duration heavy rainfall to provinces along its path, including Hebei, Henan, Shandong, and Jiangsu (Fig. 1a).

At around 12:00 Beijing Time (BT) on June 13, multiple convective cells were sequentially initiated in northern Henan and the eastern part of northwestern Shandong. As these cells moved eastward, they gradually organized into the first squall line (hereinafter referred to as Squall Line I). This squall line reached a maximum length of approximately 750 km and persisted for about seven hours, from approximately 14:00 to 20:00 BT, traversing most of central and eastern Shandong. The second squall line (hereinafter referred to as Squall Line II) formed in southern Hebei at 16:30 BT and moved eastward, affecting only southern Hebei and northwestern Shandong. Its echoes weakened and dissipated around 20:00 BT, lasting 3.5 hours with a maximum length of approximately 200 km.

During the event, a total of 32 station reports documented thunderstorm gales of force 10 or higher. The highest wind speed recorded at regional stations was 29.4 m/s (force 11, observed at Jiaolong, Linshu, at 19:07 BT). In the eastern Shandong Peninsula, encompassing Qingdao, Yantai, and Weihai, 104 stations experienced heavy rainfall, with a maximum accumulated precipitation of 156.4 mm. The maximum hourly rainfall intensity reached 103.4 mm (observed at Sanshandao, Laizhou, between 15:00 and 16:00 BT). Additionally, hail occurred in northwestern Shandong and central Shandong cities such

as Dongying, Binzhou, Dezhou, Jinan, and Weifang, causing substantial damage. The key stations involved in this study are indicated in Fig. 1b.

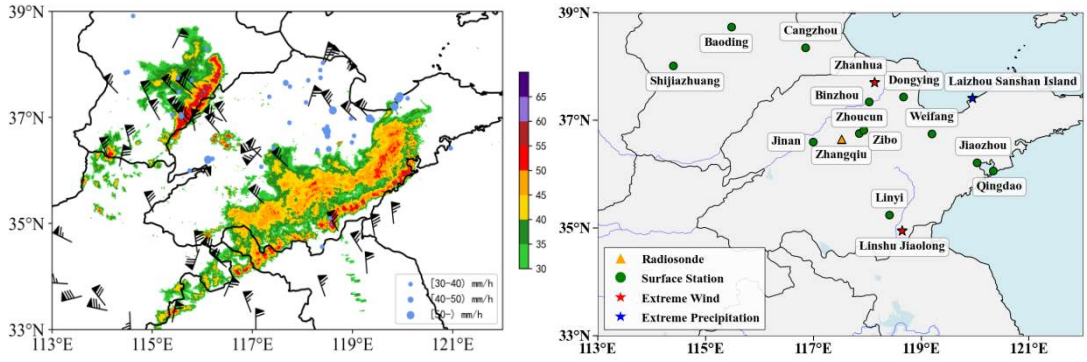


Figure 1

The position of the Squall Line at 19:00 BT 13 June 2022 (a, color shaded: the composite reflectivity above 30 dBZ, wind barb: gusts greater than force 10, green dots: 1-hour precipitation above 30 mm/h) and the locations of the major stations referenced in this study (b)

4. Circulation Background for the Squall Lines

At 08:00 BT on June 13, the 500 hPa center of the Northeast China Cold Vortex was situated in the central-eastern part of Inner Mongolia (near 46°N), with a cold core of -16 °C. A secondary cold center was present at the junction of Hebei, Henan, and Shanxi, and much of southern North China lay within a dry zone (Fig. 2a). At 850 hPa, a well-defined warm tongue extended from northwestern Henan to northwestern Shandong, vertically superimposing with the 500 hPa cold vortex trough. This created an "upper-cold, lower-warm" thermally unstable stratification. Western Shandong was ahead of the 850 hPa trough and under the influence of a low-level southwest jet, experiencing significant warm and moist advection (Fig. 2b). The mid-to-upper-level dry and cold advection overlapped with the lower-level warm and moist advection, resulting in a large vertical temperature lapse rate. The temperature difference between 850 hPa and 500 hPa over southern North China reached 30-35 °C. At 925 hPa, a warm ridge extended into northwestern Shandong, with specific humidity exceeding 10 g/kg.

During the daytime on June 13, due to the combined effects of solar radiation heating and warm and moist advection, the surface temperature at the junction of Shandong and Hebei rose rapidly. The maximum afternoon temperature generally exceeded 30 °C, promoting the continuous accumulation of unstable energy in the boundary layer. From 08:00 BT to 20:00 BT, as the 500 hPa transverse trough moved southward, strong positive vorticity advection ahead of the trough caused a decrease in low-level pressure, and a surface cyclonic circulation developed. Observations at 11:00 BT revealed that a closed surface low-pressure center (with a central pressure of about 1002 hPa) had formed in southwestern Shandong. By 14:00 BT, a "λ-shaped" wind shear structure appeared in central Shandong, and northwestern Shandong was located in the convergence zone at the top of the surface inverted trough. Meanwhile, as the upper-level cold vortex continued to rotate, a second short-wave trough split and moved southward into the central-southern part of Hebei by 15:00 BT (Fig. 2c), further enhancing the dynamic lifting conditions in the region. This synergy between the upper- and lower-level systems, along with the previously accumulated thermal instability energy, provided highly favorable environmental conditions for severe convective weather.

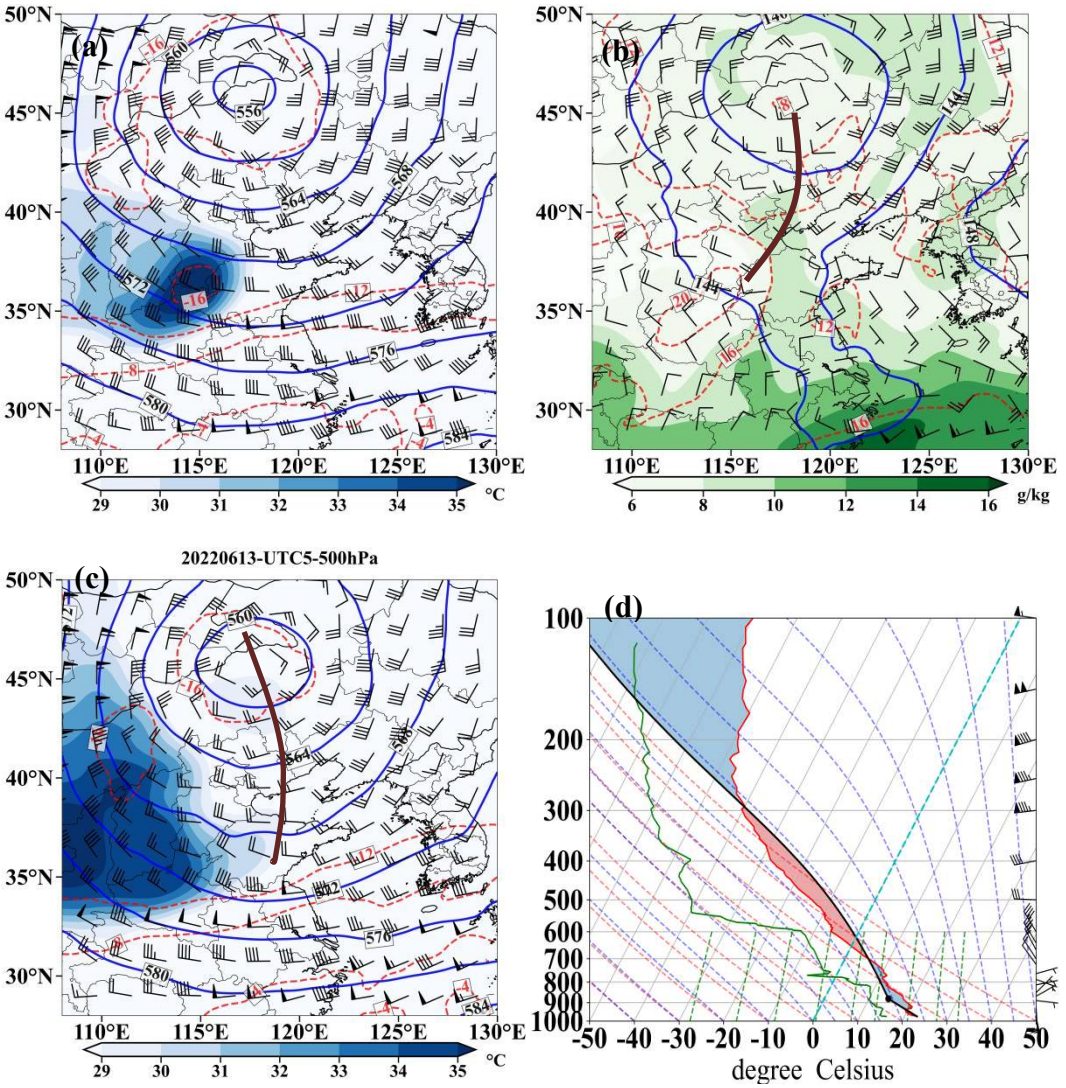


Figure 2

Synoptic situation at (a) 500 hPa at 08:00 BT, (b) 850 hPa at 08:00 BT, and (c) 500 hPa at 15:00 BT on 13 June 2022 (Blue solid lines: geopotential height, unit: dagpm; Red dashed lines: temperature, unit: °C; Brown solid lines: trough lines or shear lines; Shading at 500 hPa: temperature difference between 850 hPa and 500 hPa, unit: °C; Shading at 850 hPa: specific humidity at 850 hPa, unit: g/kg), and (d) Zhangqiu sounding at 08:00 BT

To quantitatively describe the favorable environmental conditions, key physical parameters from the Zhangqiu sounding at 08:00 BT on June 13 (Fig. 2d) are summarized in Table 1. The analysis shows strong thermal instability in the atmosphere, characterized by high CAPE values and weak convective inhibition, with all instability indices indicating significant convective potential. As Fig. 2d depicts, the vertical humidity distribution exhibits moist conditions in the mid-to-low levels and a dry layer in the mid-levels, which is conducive to severe convection development and downdraft enhancement. The vertical wind shear is strong, promoting convective organization. The stratification curve displays a typical “trumpet-shaped” pattern, with lapse rates approaching the dry adiabatic lapse rate between 750-600 hPa and 950-800 hPa. This configuration facilitates the entrainment of mid-level dry air into the convective system, leading to downdraft formation through intense evaporative cooling. This, in turn, generates a rapidly moving strong cold pool and significantly increases the potential risk of surface gales.

Table 1

Key physical parameters from the Zhangqiu sounding at 08:00 BT on 13 June 2022

Parameter	Value	Significance
CAPE	942.6 J/kg (approximately 2300 J/kg after correction)	Abundant energy, strong convective potential
CIN	0 J/kg	No convective inhibition, favorable for initiation
K index	28 °C	Strong thermal instability
SI index	-2.66 °C	
LI index	-4.3 °C	
0°C layer height	Approximately 3.6 km	Favorable for hail growth
-20°C layer height	Approximately 6.3 km	
0-6 km vertical wind shear	Approximately 15 m/s	Favorable for convective organization and maintenance
0-3 km vertical wind shear	Approximately 14.8 m/s	

5. Initiation Organization of Two Squall Lines

5.1. Development and Evolution of Squall Line I

On June 13, between 08:00 and 12:00 BT, a pronounced shear line was observed on the 850 hPa isobaric surfaces (brown line in Fig. 2b). This shear line triggered severe convective echoes that initially developed on the western side of Bohai Bay, and subsequently moved eastward and organized into a band along the shear line. Surface observations indicated a persistent mesoscale vortex from southern Hebei to Shandong, moving slowly eastward and southward, with convergence lines on its northeastern and southwestern sides.

At 10:50 BT, the severe convective cluster over Bohai Bay began to affect the northwestern coastal area of Shandong (Figs. 3a, b). A significant surface cold pool and gust front system developed on the storm's southwestern side, with the cold pool center temperature below 20 °C and a maximum temperature gradient of 10 °C over 10 km. Subsequently, this gust front encountered near-surface southerly winds, creating a region with wind speed differences, wind direction convergence, and backward propagation, leading to enhanced convergence and the formation of a mesoscale convergence center (labeled D in Figs. 3a, b). Calculations from surface automatic weather station data showed that the convergence center intensity reached -20×10^{-5} s^{-1} at 11:30 BT (Fig. 4a) and further intensified to -40×10^{-5} s^{-1} by 12:00 BT ahead of the cold pool (Fig. 4b).

Under the combined effects of surface warming (surface temperatures around 30 °C in unaffected areas, Fig. 3b), the gust front formed by strong storm outflow (Figs. 3c, 3d), and the mesoscale convergence center, multiple convective cells were triggered around Binzhou and Dongying in northwestern Shandong around 12:00 BT (with a recorded instantaneous maximum wind speed of 32.2 m/s at Zhanhua, Dongying). By 13:00 BT, these cells merged to form a southwest-northeast-oriented severe thunderstorm band with a maximum reflectivity of 68 dBZ. As the surface convergence line moved eastward, the thunderstorm's cold pool continuously expanded, with its temperature gradient and convergence zone extending further southward, continuously triggering new convection (Fig. 3b, Figs. 4a-4d).

Additionally, the dynamic lifting effects of the southward-moving low-level shear line and the convergence line on the southwestern side of the mesoscale vortex triggered multiple convective storms over land from Puyang (Henan) to Liaocheng (Shandong) to Jinan (Shandong). These storms gradually

organized along the southwestern convergence line and began merging around 13:30 BT, eventually evolving into a linearly arranged convective system. By approximately 14:00 BT, the convective system from Bohai Bay merged north-south with the inland linear convective system extending from Puyang (Henan) to Liaocheng (Shandong) to Jinan (Shandong), forming Squall Line I, which consisted of multiple individual storm cells.

By 15:00 BT, Squall Line I moved eastward to the Weifang area, evolving into a trailing stratiform squall line, maintaining a speed of approximately 40 km/h. It continued eastward and southward, exiting Shandong and entering Jiangsu by 20:00 BT. This squall line had a long lifespan and wide impact range, reaching a maximum length of approximately 750 km and lasting for 7 hours, with severe convective weather, including hail and thunderstorm gales, occurring along its path.

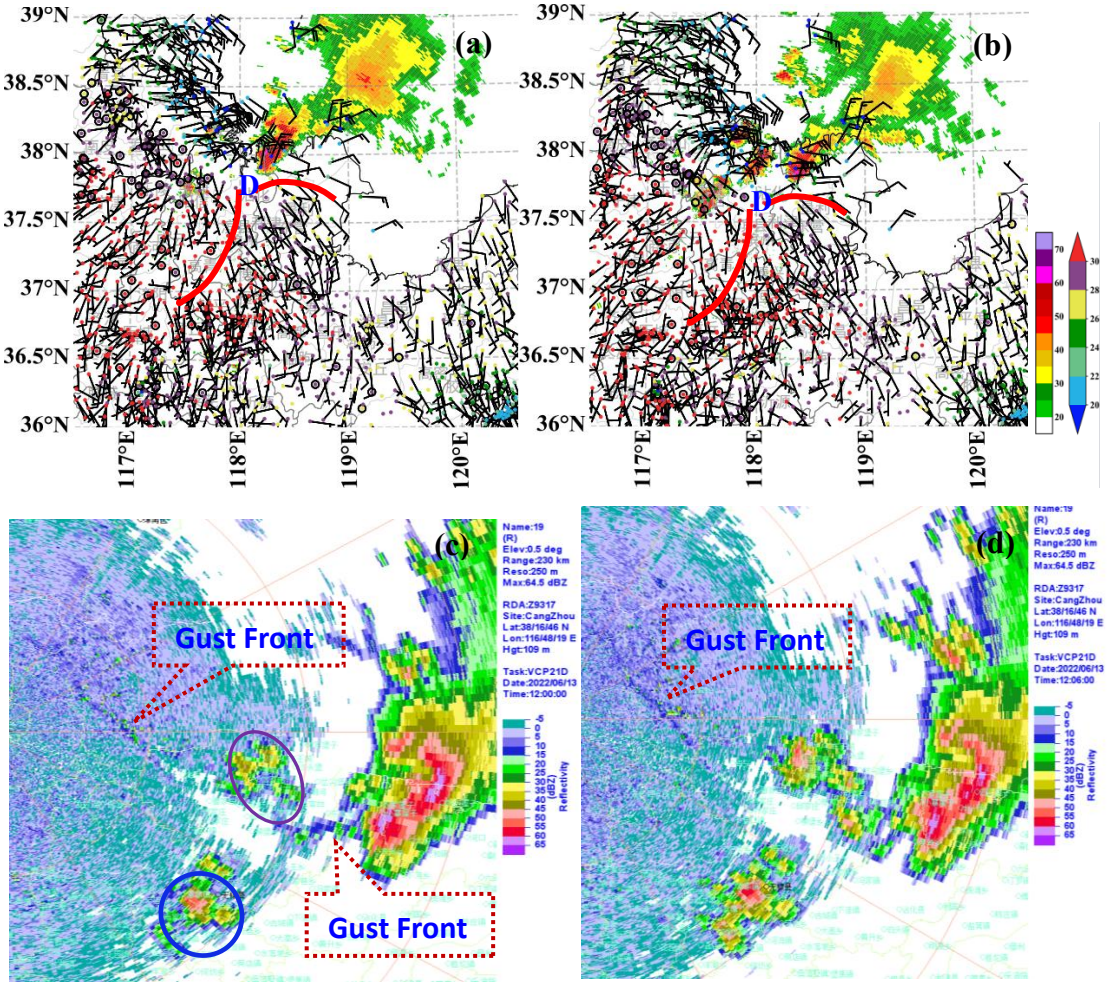


Figure 3

Automatic weather station data (wind barbs), temperature (dots) overlaid with radar composite reflectivity (D denotes mesoscale vortex; red lines denote mesoscale convergence lines) at (a) 12:00 BT, (b) 12:30 BT, 0.5° elevation reflectivity factor from Cangzhou radar (c) 12:00 BT, (d) 12:06 BT on 13 June 2022

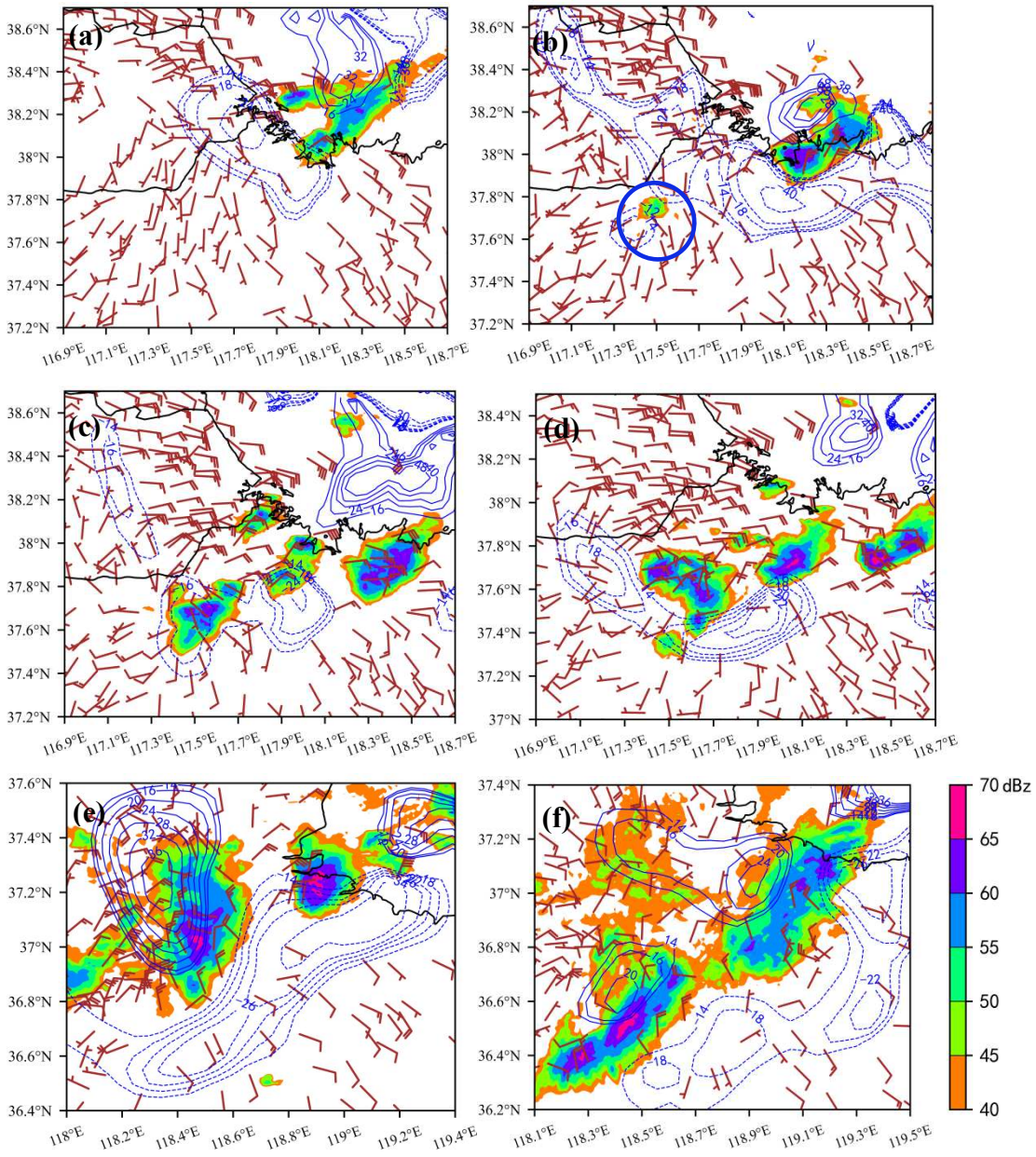


Figure 4

Automatic weather station gust (wind barbs), divergence (blue contours), and radar composite reflectivity (shaded) at (a) 11:30, (b) 12:00, (c) 12:30, (d) 13:00, (e) 15:00, (f) 16:00 on 13 June 2022

It can be seen that the formation of Squall Line I resulted from the merging of two convective systems: the coastal segment originated from a convective system that developed over Bohai Bay on the morning of June 13 (figure omitted) and subsequently propagated in a southwestward (inland) retrograde manner; the inland segment consisted of newly formed convective cells spanning from Puyang in Henan to Liaocheng and Jinan in Shandong, which organized and intensified along the convergence line. The triggering mechanisms of these two segments displayed distinct dynamic characteristics. The southward shift of the low-level shear line, influenced by the cold vortex, created favorable lifting and triggering conditions, while the mesoscale surface vortex and its associated flanking convergence lines played a pivotal role in determining the sites of convective initiation and organization. Additionally, the interaction between the gust front and the southerly wind within the warm sector persistently enhanced convergence.

Ultimately, under the organizing influence of the convergence line, the two segments merged, giving rise to the quasi-linear Squall Line I. This evolutionary process comprehensively illustrates the significant contributions of multi-scale systems, including synoptic-scale shear lines, mesoscale vortices, and storm-scale cold pools, to the initiation and organization of Squall Line I.

5.2. Development and Evolution of Squall Line II

Squall Line I had a clear synoptic-scale triggering system, whereas Squall Line II formed under markedly different conditions, dominated by upper-level northwesterly flow (Fig. 2c) and lacking organized systematic lifting mechanisms such as low-level shear lines. This explains the tendency for such systems to be missed in operational forecasting. The triggering mechanisms of Squall Line II were as follows: initial convection occurred around noon, with significant radiation-induced warming over the Shanxi Plateau (surface maximum temperatures reaching 28 °C, exceeding the convective temperature of 27.8 °C). Consequently, under the influence of the terrain, scattered thermal convection was triggered in the mountainous area during the afternoon, moving eastward into the Hebei Plain under the steering of the northwesterly flow.

After the passage of Squall Line I, the convective available potential energy (CAPE) over the Hebei Plain briefly depleted but rapidly rebuilt between 14:00 and 15:00 BT under the mountainous area's thermal effect, with hourly ERA5 data indicating an increase of over 700 J/kg per hour, providing favorable conditions for the subsequent development and organization of Squall Line II. Additionally, the evolution of the specific humidity field was closely related to the development process of the squall lines, with a distinct moisture gradient zone ahead of Squall Line II (Fig. 5a, b) being formed by the convergence and concentration of low-level moisture transport. The initiation of Squall Line II under weak synoptic-scale forcing conditions exhibited three key characteristics: terrain-induced thermal forcing over the plateau triggered initial convection; rapid accumulation of unstable energy occurred over the plain area; and the formation of a moisture frontal zone was associated with the concentration of low-level moisture transport. Therefore, for systems lacking distinct dynamic triggering mechanisms, particular attention should be paid to local moisture boundaries, thermal conditions, and energy characteristics.

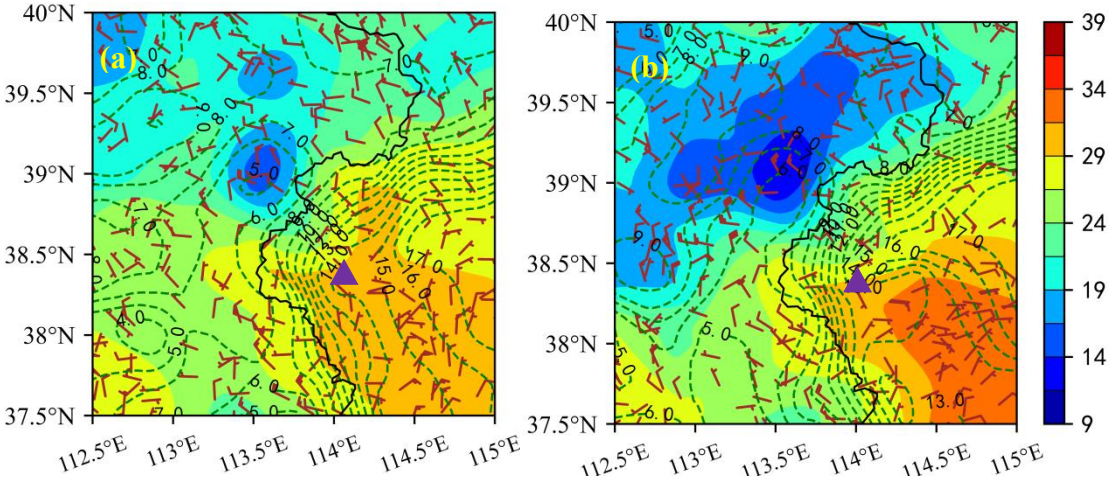


Figure 5

Distributions of wind, temperature (shaded), and dew point temperature (green dashed contours, °C) at (a) 14:00 BT, (b) 15:00 BT on 13 June 2022

At 15:00 BT, southern North China was controlled by upper-level northwesterly flow with a lower-level warm ridge, re-establishing unstable stratification characterized by cold and dry air aloft and warm and moist air near the surface. The surface wind field, with easterly wind at the top of the low-pressure system, northerly wind ahead of the surface cold front, and terrain-induced convergence, constituted a dynamic field favorable for the rapid organization of Squall Line II (Fig. 6). To be specific, after initial thunderstorms moved down from the eastern Taihang Mountains, their northerly outflow formed a distinct convergence line with the easterly wind on the western coast of the Bohai Bay (figure omitted). As the easterly flow from the Bohai Sea advanced westward, the easterly component in the lower levels significantly intensified, deflecting under topographic forcing when approaching a direction nearly perpendicular to the Taihang Mountains, forming a stable convergence line at the mountain front, which was clearly identified from Cangzhou Doppler radar reflectivity (Fig. 10) and surface automatic weather station winds (Fig. 6). The radar data showed a continuous band of enhanced reflectivity along the eastern slope of the Taihang Mountains, collocated with a surface wind shift from easterly to northerly. This convergence feature was well captured by both the radar and surface observations. After moving down from the mountains, the thunderstorm belt rapidly developed near this convergence line, with its morphology generally consistent with the orientation of the convergence line.

In addition, the surface cold front influenced the development of Squall Line II. During its initial stage (16:30–18:00 BT), a region of large frontogenesis function values existed near the newly generated convection. Subsequently, the convective belt developed parallel to the frontogenesis zone (Fig. 6). The strong frontogenesis zone in the northern part continuously triggered new convection, facilitating the formation and development of a bow echo structure in southern Hebei, while convection remained scattered in the southern part where frontogenesis was weaker. Squall Line II formed around 16:30 BT in the Baoding–Shijiazhuang area of southern Hebei. After entering the mature stage (18:00–19:00 BT), it moved eastward into northwestern Shandong. Although the reflectivity intensity remained at 60 dBZ and the movement speed accelerated to 70 km/h, thermal conditions significantly deteriorated, manifested by a notable decrease in CAPE and a decline in the temperature gradient. During the decay and dissipation stage (19:00–20:00 BT), as the inflow ahead of the system turned to northerly, the vertical wind shear weakened, and the cold pool intensity decreased. After entering the area previously affected by Squall Line I (with surface temperatures of 16-19 °C), the atmospheric energy conditions failed to recover in time, resulting in insufficient thermal conditions for the development of Squall Line II, and the system rapidly dissipated, with its entire lifespan lasting only about 3.5 hours.

This process reveals the development characteristics of a short-lived squall line under weak synoptic-scale forcing: its initial triggering relied on significant terrain-induced thermal forcing over the plateau and low-level dynamic convergence; during the development stage, the system's organization process was primarily dominated by low-level frontogenetic dynamic forcing; and the system's maintenance was constrained by insufficient local unstable energy supply. These characteristics contrast sharply with the prolonged maintenance of the long-lived Squall Line I, which resulted from the synergistic effects of multi-scale systems.

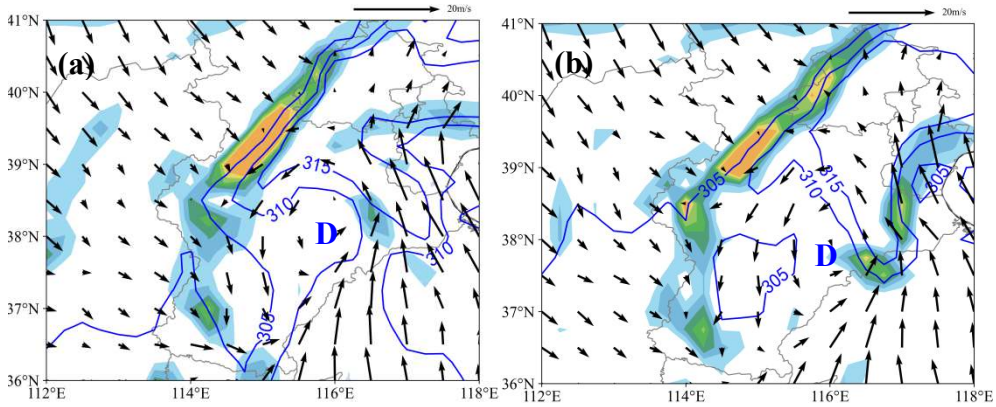


Figure 6

Analysis of the 925 hPa wind field superimposed with frontogenesis (shaded, 10^{-9} K/(m·s)) and equivalent potential temperature (contoured, K) and wind at (a) 13:00 BT, (b) 14:00 BT on 13 June 2022

5.3. Maintenance Mechanism of Long-Lived Squall Line I

According to the RKW theory, when the propagation speed of the cold pool boundary approaches the low-level environmental vertical wind shear (i.e., their ratio approaches 1), the negative vorticity generated by the cold pool and the positive vorticity generated by the low-level vertical wind shear reach an approximate equilibrium. This equilibrium results in the strongest updraft at the leading edge of the cold pool, promoting the stable maintenance and sustained development of the squall line system. Cold pools are highly sensitive to cloud microphysical processes (Pu et al., 2019), which can modulate their intensity and longevity through evaporative cooling and precipitation loading. Furthermore, the relative strength ratio between the cold pool and the vertical wind shear also affects the organizational structure and lifespan of convective systems (Weisman & Rotunno, 2004). Analysis of the surface pressure and temperature fields at 18:00 BT on June 13 revealed a significant thunderstorm high pressure system and a strong cold pool behind the squall line, indicating substantial cold pool intensity. Meanwhile, the 0-3 km vertical wind shear was oriented from northwest to southeast, nearly perpendicular to the southwest–northeast orientation of the squall line, a configuration that satisfies the fundamental conditions of the RKW theory.

As demonstrated in Table 2, during the initial development stage of Squall Line I (12:00–13:00 BT), the ratios of cold pool propagation speed to low-level vertical wind shear were 0.91 and 0.88, respectively. This near-equilibrium state provided favorable conditions for the rapid development of the severe convective system, gradually transforming it into a typical bow echo structure. As the system entered the mature stage (14:00-17:00 BT), the cold pool intensity continued to strengthen. Its boundary propagation speeds (20.73 m/s at 14:00 BT, 21.89 m/s at 15:00 BT, 17.25 m/s at 16:00 BT, and 18.63 m/s at 17:00 BT) all exceeded the vertical wind shear values at the corresponding stations (Weifang Station and Jiaozhou Station). This cold-pool-dominated dynamic structure caused the stratiform clouds within the convective system to tilt significantly upstream, forming a typical bow echo feature bulging southeastward. When the system entered the decay stage (after 17:00 BT), the ratio of cold pool propagation speed to wind shear at Weifang Station increased to above 1.55. This gradually imbalanced state made it difficult to maintain the horizontal vorticity, and radar echoes indicated that the system began to weaken, with the maintenance mechanism further disrupted. Around 19:00 BT, after the main body of the squall line moved offshore from the Huangdao area of Qingdao, although the cold pool

remained relatively strong, the system rapidly dissipated within half an hour due to a sharp decrease in environmental vertical wind shear.

In summary, the prolonged maintenance of Squall Line I (approximately 7 hours) was closely related to the ratios of cold pool propagation speed to environmental vertical wind shear ranging from 0.88 to 1.63. In contrast, the ratios for Squall Line II remained within this range for a shorter period, lasting only about 3 hours, resulting in a significantly shorter lifespan for the system. It can be concluded that the relative strength relationship between the cold pool and low-level vertical wind shear is a key factor determining the lifespan and organizational degree of squall lines. When the ratio deviates from the ideal equilibrium state, the development of the system is significantly suppressed.

Table 2

Ratio of cold pool boundary propagation velocity to low-level vertical wind shear

Time(BT)	Δp(hPa)	$\bar{\rho}(kg/m^3)$	$C(m/s)$	$\Delta U_{0\sim3km}(m/s)$	$C/\Delta U_{0\sim3km}$
12:00	1.6	1.20	16.32	18 (Dongying)	0.91
13:00	1.2	1.20	14.14	16 (Dongying)	0.88
14:00	2.6	1.21	20.73	16 (Weifang)	1.30
15:00	2.9	1.21	21.89	16 (Weifang)	1.37
16:00	1.8	1.21	17.25	14 (Weifang)	1.23
17:00	2.1	1.21	18.63	12 (Jiaozhou)	1.55
18:00	2.3	1.20	19.58	12 (Jiaozhou)	1.63

6. Analysis of Extreme Gale Causes

The mechanisms behind the extreme gales produced by squall lines are intricate, primarily including cold pool outflows resulting from strong downdrafts reaching the surface, rear-inflow jets associated with storm-scale structures like bow echoes or mesocyclones, and the downward transport of upper-level horizontal momentum. These mechanisms interact differently under various environmental backgrounds and can combine nonlinearly, ultimately leading to extreme surface gales. On June 13, 2022, two squall lines impacted Shandong. Squall Line I triggered extreme gales of force 8–10, with local force 11, across most of Shandong (excluding the peninsula region), mainly from 14:00 to 20:00 BT. Squall Line II affected Shandong from 19:00 to 21:00 BT, generating localized extreme gusts of force 11. Despite both causing extreme gales, their dominant mechanisms differed significantly due to variations in environmental conditions and system structures.

Between 15:00 and 16:00 BT, Squall Line I primarily affected the Zibo and Linyi areas of Shandong, causing widespread thunderstorm gales, localized hail, and short-duration heavy rainfall. A key prerequisite for the formation of a strong cold pool was the environmental stratification conducive to strong evaporative cooling, characterized by mid-level dry air intrusion and intense evaporative cooling effects. The Zhangqiu sounding at 08:00 BT on June 13 revealed a deep dry layer between 600 and 750 hPa with a lapse rate close to the dry adiabatic rate, while specific humidity in the lower levels (850 hPa and below) generally exceeded 8-10 g/kg. This “dry aloft, moist below” unstable stratification was ideal for generating a strong cold pool. When the updraft of Squall Line I entrained mid-level dry air into the cloud, intense evaporative cooling was induced, which significantly enhanced the negative buoyancy of

the downdraft. The cold air from evaporative cooling accumulated near the surface, forming a strong thunderstorm high pressure and a horizontal pressure gradient, which drove powerful outflow gales.

From the perspective of system structure, Squall Line I evolved into a trailing stratiform squall line during its mature stage (Fig. 1). This structure facilitated continuous evaporation and accelerated descent of downdrafts within the extensive stratiform region, resulting in a deep and intense cold pool. As listed in Table 2, the cold pool boundary propagation speed remained mostly above 16 m/s throughout its lifespan, even exceeding 20 m/s during the mature stage, indicating its extreme intensity. The evolution of cold pool intensity in this region was also evident in the vertical structure. From 12:00 BT onward, cooling occurred in the convective region below 900 hPa (Fig. 7a). By 13:00 BT (Fig. 7b), the cold pool (red box) with a core temperature as low as 18 °C descended to the surface, with its intensity and extent increasing simultaneously, causing surface temperatures to drop to 18 °C. This intense cold pool downdraft extended up to 850 hPa and encountered the southerly warm and moist airflow on the eastern side of the system, forming strong low-level convergence and lifting. This not only provided dynamic support for the maintenance of Squall Line I but also further promoted the intensification and propagation of the cold pool. Thus, the core driving force of the extreme gales generated by Squall Line I was the large-scale, high-intensity cold pool and its outflow.

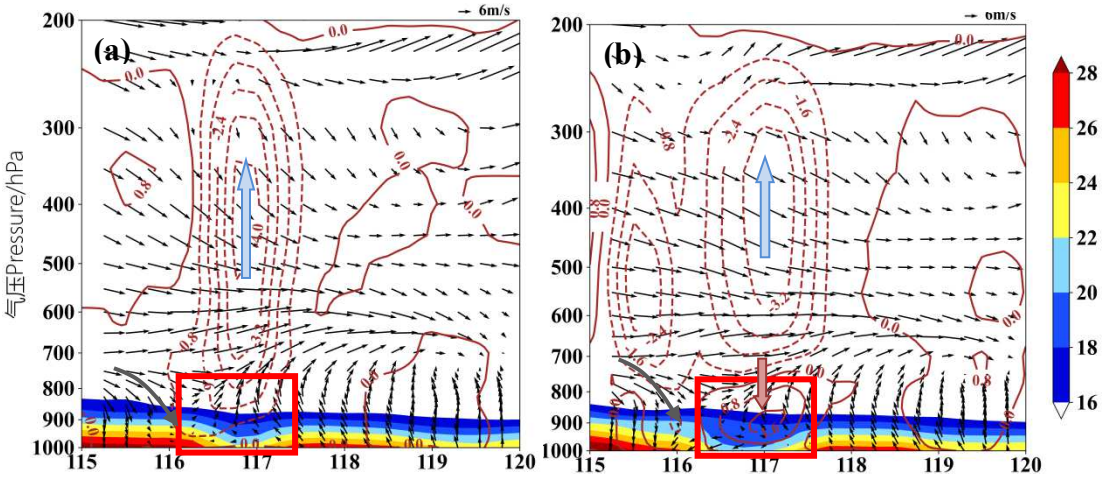


Figure 7

Vertical profile distribution along 37.75 °N: vertical velocity (red contours, Pa/s), wind field (arrows, m/s), superimposed temperature (shaded, °C) at (a) 12:00 BT, (b) 13:00 BT on 13 June 2022

Subsequently, Squall Line I continued to intensify and move eastward, with the cold pool range, intensity, and the extent of thunderstorm gales further expanding. Hourly automatic weather station data at 15:00 BT (Fig. 8a) showed that the thunderstorm gales were predominantly northerly. At 15:00 BT, the central pressure of the thunderstorm high pressure was below 1003 hPa, and the strong cold pool, with a central temperature of 17 °C caused by convective precipitation, had an area with a 1-hour temperature decrease below -12 °C located near the thunderstorm high pressure center, where the temperature decrease center was below -15 °C. From the surface wind field, it can be seen that a surface low-pressure center existed ahead of the thunderstorm movement direction, with a central pressure of 1000 hPa, and the strong outflow ahead of the storm was located between the thunderstorm high pressure and the low-pressure. The thunderstorm high pressure caused by the small-scale cold pool and the

localized small low pressure formed a strong pressure gradient, enhancing the intensity of surface gales. In addition, a temperature frontal zone formed between the cold pool center and the warm region (30 °C) in central Shandong that was unaffected by convection, with temperatures within the cold pool being more than 10 °C lower than those ahead of it. Widespread convective gales mainly occurred within the cold pool ahead of and behind the thunderstorm high pressure. Dew point temperatures also differed between the areas ahead of and behind the strong cold pool (the black numbers in Fig. 8a represent the temperature-dew point spread). For example, Linzi and Guangrao Port, two representative stations within the cold pool region, both recorded a 1-hour temperature decrease exceeding 12 °C and sustained gales of force 8 or above (Fig. 8a). By 16:00 BT (Fig. 8b), the cold pool intensity weakened, and the pressure gradient between the high and low pressures decreased. Although thunderstorm gales still occurred, both the number of stations reporting thunderstorm gales and the wind intensity were significantly reduced compared to the previous hour. Moreover, wind profiler data demonstrated no significant characteristics of downward momentum transport.

Therefore, the extreme gales generated by Squall Line I were primarily outflow gales driven by the strong pressure gradient associated with a large-scale, high-intensity cold pool. These gales were strong and relatively uniformly distributed, highly consistent with the orientation of the gust front at the leading edge of the cold pool.

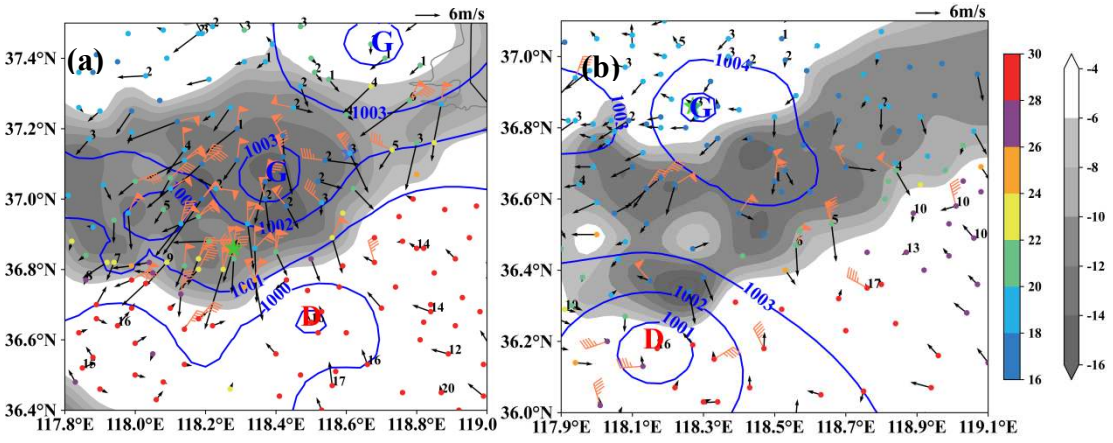


Figure 8

High-density automatic weather station data (blue solid contours: sea level pressure, dagpm, wind barbs: gusts with wind speed ≥ 17 m/s within 1 hour, arrow: automatic station wind field, colored dots: temperature, ℃, shadow: 1 hour temperature change, ℃, number: temperature dew point difference, ℃, ★ Linzi, ★ Guangrao Port (a) 15:00 BT, (b) 16:00 BT on 13 June 2022

Squall Line II was triggered in the afternoon and had a shorter lifespan and a smaller cold pool extent. Although its environmental energy (CAPE) rebuilt rapidly, both the thickness and intensity of the dry layer were lower than those during the initial stage of Squall Line I. The Cangzhou sounding at 16:00 BT, calculated using ERA5 data (Fig. 9), revealed that although this region still possessed high instability energy (1507 J/kg) and a dry layer in the mid-levels, the mid-level atmospheric humidity was relatively higher compared to the Zhangqiu sounding at 08:00 BT. This implies that the potential for driving the cold pool solely through evaporative cooling in Squall Line II was weaker than that in Squall Line I. Under these circumstances, system structure and dynamic processes became key factors in the generation of high winds.

Radar echoes (Fig. 10) indicated that Squall Line II rapidly developed a bow echo structure in southern Hebei, with more pronounced bow-shaped characteristics. The bow echo is one of the most favorable structures for producing extreme gales, with its core mechanism being a strong rear-inflow jet. During the development of Squall Line II, influenced by the configuration of the upper-level northwesterly flow and the low-level wind field, the environmental 0-3 km vertical wind shear reached 12-14 m/s, which favored the establishment and maintenance of the rear-inflow jet. This rear-inflow jet transported high-momentum air from the upper levels into the storm interior and accelerated the downdraft through processes such as precipitation drag and dynamic pressurization. In contrast to Squall Line I, where evaporative cooling dominated, the contribution of dynamic forcing to the downdraft in Squall Line II was more prominent. After reaching the surface, this strong downdraft combined with the strong environmental wind behind the storm, generating localized surface gales. Furthermore, a mesoscale vortex existed ahead of Squall Line II, which favored dynamic pressure reduction, further enhancing the local wind intensity and resulting in a more concentrated distribution of high winds.

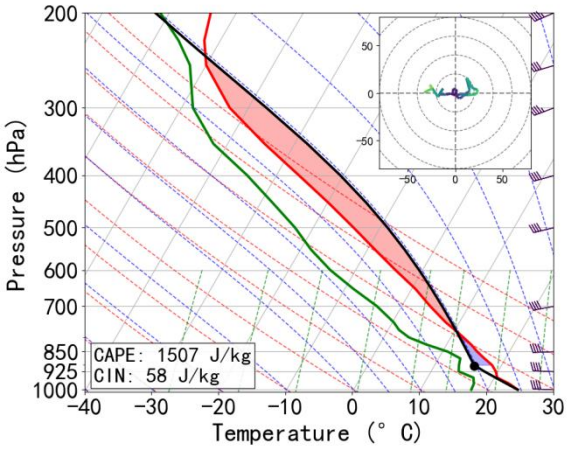


Figure 9

Reanalyzed sounding at Cangzhou at 16:00 BT on 13 June 2022

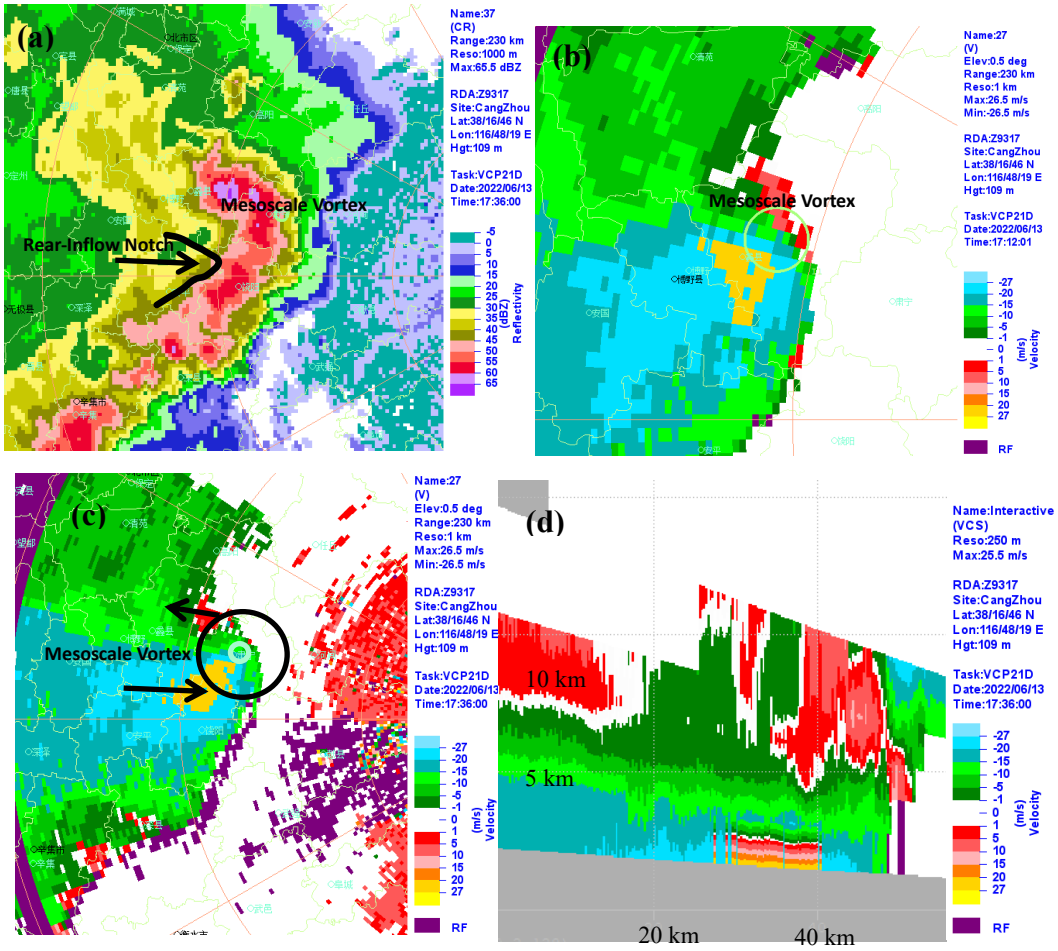


Figure 10

Cangzhou Radar's 17:36 BT composite reflectivity (a), 17:12 BT radial velocity (b), 17:36 BT radial velocity (c), and 17:36 radial velocity profile (d) on 13 June 2022

The temporal evolution of surface meteorological elements at Zhoucun Station in Zibo, which was affected by Squall Line II (Fig. 11), was analyzed. When the extreme gale occurred at this station, it was located ahead of the thunderstorm high pressure. The temperature dropped by approximately 13 °C between 17:45 and 18:15 BT, indicating the presence of cold advection aloft, corresponding to the cold pool generated by the convective storm and the downdraft process behind the storm. Corresponding to the temperature drop, the pressure exhibited a fluctuating increase. Near the surface, northerly gales prevailed. After the wind speed at this station reached its peak, the surface pressure indicated a slight decrease, which may have been related to the mesoscale cyclone ahead of the squall line extending downward to the lower levels. During this period, the maximum surface wind speed remained above 18 m/s. Subsequently, as the convective cold pool advanced further, the pressure continued to rise to 1001.6 hPa, indicating that the influence of the main cold pool occurred later. Notably, the precipitation during this period was not intense, and the gravitational drag effect of the precipitation mass was not significant.

In conclusion, the extreme gales caused by Squall Line II resulted from the combined and superimposed effects of the mesoscale vortex within the bow echo and the rear-inflow jet, with the dominant mechanism focusing more on the dynamic processes and mesoscale structures within the storm interior.

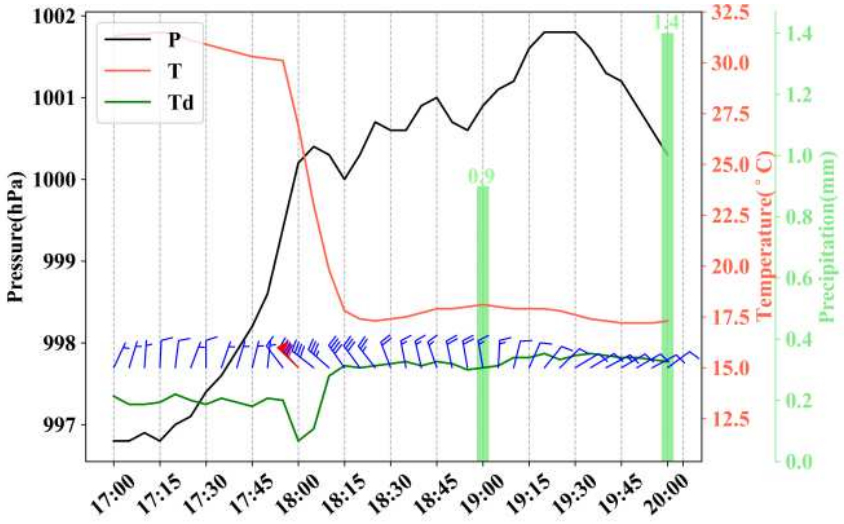


Figure 11

Evolution of meteorological elements at Zhoucun automatic station in Zibo, Shandong, on 13 June 2022 (blue solid Line: sea level pressure; red solid line: temperature; green solid line: dew point temperature, wind barb: maximum gusts, bar chart: 1-hour precipitation)

7. Conclusion

Through an observational and diagnostic analysis of multi-source data, including ERA5 reanalysis and radar observations, this study investigated a double-squall-line event that occurred in southern North China and the Huanghuai region on June 13, 2022. The focus was on the circulation background, initiation and organization mechanisms, maintenance mechanisms, and mechanisms underlying extreme gales. The main findings are as follows:

This severe convective weather event in southern North China and the Huanghuai region occurred under the background of a cold vortex. Strong thermal instability was created by the overlap of dry and cold advection in the mid-to-upper levels with warm and moist advection in the lower levels, providing favorable thermodynamic conditions for convective initiation. Additionally, abundant low-level moisture, significant vertical wind shear, and strong afternoon surface heating collectively established an optimal environmental field for the initiation and organized development of the squall lines.

The initiation and organization mechanisms of the two squall lines differed significantly. Squall Line I appears to have been governed by the synergistic effects of multi-scale systems: the southward movement of a synoptic-scale low-level shear line provided initial lifting conditions; a mesoscale surface vortex and its flanking convergence lines determined the locations of convective initiation and organization; and the interaction between the storm-scale gust front and warm and moist air continuously reinforced convergence. Ultimately, Squall Line I formed through the merger of two convective systems from coastal and inland sources. In contrast, Squall Line II exhibited localized initiation characteristics under weak synoptic-scale forcing, triggered by thermal forcing over the Taihang Mountains in the afternoon. Subsequently, as the convection moved downhill, the convergence line formed by the interaction between low-level easterly winds and the terrain, along with low-level frontogenetic dynamic forcing, jointly dominated the organization of convection and the eventual formation of the squall line.

The interaction between the cold pool and vertical wind shear was crucial for the differences in lifespan and intensity between the two squall lines. Squall Line I maintained for up to 7 hours, benefiting from a sustained near-equilibrium state between the cold pool boundary propagation speed (C) and the 0-3 km vertical wind shear ($\Delta U_{0\text{-}3\ km}$), with ratios ranging from 0.88 to 1.63, consistent with the ideal conditions for squall line maintenance described by the RKW theory. In contrast, Squall Line II maintained balance for a shorter period and moved into an area previously affected by Squall Line I, where energy had not fully recovered, leading to a rapid imbalance in the $C/\Delta U_{0\text{-}3\ km}$ ratio and resulting in its short lifespan and limited development.

The physical mechanisms responsible for the extreme gales generated by the two squall lines differed. The gales produced by Squall Line I were closely associated with a large-scale, high-intensity cold pool. The intrusion of mid-level dry and cold air formed a deep and strong cold pool through intense evaporative cooling, and the outflow gales driven by the strong pressure gradient were the dominant cause of widespread gales of force 8 to 11, which were strong and relatively uniformly distributed, highly consistent with the orientation of the gust front at the leading edge of the cold pool. In contrast, the gales caused by Squall Line II were more closely related to the internal dynamic processes and mesoscale structures of the storm. The bow echo structure that developed during its evolution, combined with strong environmental vertical wind shear, organized a powerful rear-inflow jet. The strong downdraft under dynamic forcing transported upper-level momentum downward, serving as the core mechanism for the localized extreme gusts, with the distribution of thunderstorm gales being relatively concentrated.

This study reveals the complex physical mechanisms underlying the successive initiation of two squall lines under the influence of a cold vortex and clarifies the differences in the dominant mechanisms responsible for extreme gales between different squall line systems. These findings are significant for enhancing the understanding of the diversity of mesoscale convective systems and for improving their forecasting and early warning capabilities. The quantitative diagnostic framework established here—particularly the $C/\Delta U$ ratio and frontogenesis-based indicators—provides a basis for future observational and modeling studies of squall lines under similar cold vortex conditions.

Author Contribution Jiangshan Luo performed the formal analysis, investigation, and visualization, and wrote the original draft and revised the manuscript. Fujing Wan conceived and designed the study, curated the data, acquired the funding, administered the project, supervised the research, and reviewed and edited the manuscript. Jian Li contributed to the methodology, validated the results, and reviewed and edited the manuscript. All authors read and approved the final manuscript.

Funding

This work was supported by the Natural Science Foundation of Shandong Province (ZR2025LQX005) and the Shandong Meteorological Bureau Key Project (2025sdqxz18).

Data Availability

The data and references presented in this study were available from the corresponding author upon reasonable request.

Declarations

Conflict of interests The authors declare that they have no conflict of interests.

Publisher's Note Springer Nature remains neutral with regard to jurisdictional claims in published maps and institutional affiliations.

REFERENCES

Abramian, S., Muller, C., & Risi, C. (2022). Shear-convection interactions and orientation of tropical squall lines. *Geophysical Research Letters*, 2022(1), 49. https://doi.org/10.1029/2021GL095184

Benjamin, T. B. (1968). Gravity currents and related phenomena. *Journal of Fluid Mechanics*, 31 (2), 209-248. https://doi.org/10.1017/S0022112068000133

Carbone, R. E., Conway, J. W., Crook, N. A., & Moncrieff, M. W. (1990). The generation and propagation of a nocturnal squall line. Part I: Observations and implications for mesoscale predictability. *Monthly Weather Review*, 118, 26–49. https://doi.org/10.1175/1520-0493(1990)118<0026:TGAPOA>2.0.CO;2

Du, Y., & Chen, G. (2019). Heavy rainfall associated with double lowlevel jets over southern China. Part II: Convection initiation. *Monthly Weather Review*, 147, 543–565. https://doi.org/10.1175/MWR-D-18-0102.1

French, A. J., & Parker, M. D. (2014). Numerical simulations of bow echo formation following a squall line-supercell merger. *Monthly Weather Review*, 142 (12), 4791-4822. https://doi.org/10.1175/MWR-D-13-00356.1

Gebauer, J. G., Shapiro, A., Fedorovich, E., & Klein, P. M. (2018). Convection initiation caused by heterogeneous low-level jets over the Great Plains. *Monthly Weather Review*, 146, 2615–2637. https://doi.org/10.1175/MWR-D-18-0002.1

Hitchcock, S. M., & Schumacher, R. S. (2020). Analysis of backbuilding convection in simulations with a strong low-level stable layer. *Monthly Weather Review*, 148, 3773–3797. https://doi.org/10.1175/MWR-D-19-0246.1

Hong, X. D., Li, X. F., & Zhang, D. L. (1999). The mutual response of the tropical squall line and the ocean. *Pure and Applied Geophysics*, 155(1), 1–32. https://doi.org/10.1007/s000240050252

Huang, Y. L., Li, J., Wang, Y. L., Chen, L. F., & Pang, Y. L. (2025). Triggering and maintenance mechanisms of disastrous double squall lines in the context of a cold vortex. *Desert and Oasis Meteorology*, 19 (3), 122-131. https://doi.org/10.12057/j.issn.1002-0799.2311.27001. (in Chinese)

Liu, Q. Q., Xu, X., Zhao, K., & Zhou, A. (2023). A merger-formation bow echo caused by low-level mesovortex in South China. *Journal of Geophysical Research: Atmospheres*, 128, e2022JD037954. https://doi.org/10.1029/2022JD037954

Luo, Y., Gong, Y., & Zhang, D. L. (2014). Initiation and organizational modes of an extreme-rain-producing mesoscale convective system along a mei-yu front in East China. *Monthly Weather Review*, 142, 203–221. https://doi.org/10.1175/MWR-D-13-00111.1

Luo, Y., & Zhang, R. (2017). The Southern China Monsoon Rainfall Experiment (SCMREX). *Bulletin of the American Meteorological Society*, 98, 999–1013. https://doi.org/10.1175/BAMS-D-15-00235.1

Meng, Z. Y., Yan, D. C., & Zhang, Y. J. (2013). General features of squall lines in East China. *Monthly Weather Review*, 141 (5), 1629-1647. https://doi.org/10.1175/MWR-D-12-00208.1

Parker, M. D. (2021). Self-organization and maintenance of simulated nocturnal convective systems from PECAN. *Monthly Weather Review*, 149, 999–1022. https://doi.org/10.1175/MWR-D-20-0263.1

Peters, J. M., & Schumacher, R. S. (2014). Objective categorization of heavy-rain-producing MCS synoptic types by rotated principal component analysis. *Monthly Weather Review*, 142, 1716–1737. https://doi.org/10.1175/MWR-D-13-00295.1

Petterssen, S. (1956). Weather Analysis and Forecasting (Vol. 1). McGraw-Hill.

Pu, Z., Lin, C., Dong, X., & Krueger, S. K. (2019). Sensitivity of numerical simulations of a mesoscale convective system to ice hydrometeors in bulk microphysical parameterization. *Pure and Applied Geophysics*, 176(5), 2097–2120. https://doi.org/10.1007/s00024-018-1787-z

Reif, D. W., & Bluestein, H. B. (2017). A 20-year climatology of nocturnal convection initiation over the central and southern Great Plains during the warm season. *Monthly Weather Review*, 145, 1615–1639. https://doi.org/10.1175/MWR-D-16-0340.1

Schumacher, R. S., & Rasmussen, K. L. (2020). The formation, character and changing nature of mesoscale convective systems. *Nature Reviews Earth & Environment*, 1, 300–314. https://doi.org/10.1038/s43017-020-0057-7

Song, J., Liao, K., Coulter, R. L., & Lesht, B. M. (2005). Climatology of the low-level jet at the Southern Great Plains atmospheric boundary layer experiments site. *Journal of Applied Meteorology*, 44, 1593–1606. https://doi.org/10.1175/JAM2294.1

Trier, S. B. (2003). Convective storms: Convective initiation. *Encyclopedia of Atmospheric Sciences*, 99 (12), 560-570. https://doi.org/10.1016/B0-12-227090-8/00122-6

Wan, F. J., Sun, J. S., Sun, M., Mei, C. J., & Yang, F. (2021). Impacts of sea breeze front over Shandong Peninsula on the evolution of a squall line. *Acta Meteorologica Sinica*, 79 (5), 717-731. https://doi.org/10.11676/qxxb2021.056. (in Chinese)

Wan, F. J., Sun, M., Pang, H. J., Zhao, H. J., & Zhao, C. H. (2024). Evolution mechanism of a severe squall line triggered by the coupling of a sea breeze front and a gust front. *Journal of Tropical Meteorology*, 30 (2), 200-210. https://doi.org/10.3724/j.1006-8775.2024.018

Weckwerth, T. M., & Romatschke, U. (2019). Where, when, & why did it rain during PECAN? *Monthly Weather Review*, 147, 3557–3573. https://doi.org/10.1175/MWR-D-18-0458.1

Weisman, M. L., & Rotunno, R. (2004). "A Theory for Strong Long-Lived Squall Lines" Revisited. *Journal of the Atmospheric Sciences*, 61 (4), 361-382. https://doi.org/10.1175/1520-0469(2004)061<0361:ATFSLS>2.0.CO;2

Yan, Z. D., Wang, Z. L., & Pang, L. (2022). Study of the wind conditions in the South China Sea and its adjacent sea area. *Journal of Ocean University of China*, 21 (2), 264-276. https://doi.org/10.1007/s11802-022-4801-0

Zhang, S., Parsons, D. B., Xu, X., Sun, J. S., Wu, T. J., Abulikemu, A., Xu, F., Chen, G., Shen, W. Q., Liu, L. H., Zhang, X. D., Zhang, K., & Zhang, W. (2023). Dynamics governing a simulated bow and arrow type mesoscale convective system. *Monthly Weather Review*, 151, 603–623. https://doi.org/10.1175/MWR-D-22-0091.1

Zhao, S. N., Ma, R. Q., Sun, J. W., Li, L. S., Yuan, X. F., Liang, H., & Shi, H. Y. (2025). Characterization of cold wave paths in the Laizhou Bay area. *Journal of Ocean University of China*, 24 (4), 865-874. https://doi.org/10.1007/s11802-025-5997-6

Zhou, A., Zhao, K., Lee, W.-C., Huang, H., Hu, D., & Fu, P. (2020). VDRAS and polarimetric radar investigation of a bow echo formation after a squall line merged with a preline convective cell. *Journal of Geophysical Research: Atmospheres*, 125, e2019JD031719. https://doi.org/10.1029/2019JD031719